FUDMA Journal of Engineering and Technology
ISSN: 3092-9385
https://sites.google.com/fudutsinma.edu.ng/fjet
Volume 1, Issue 2, 2025, 806-818

Development of Free Space Optical Communication Testbed for Fog and Rain Attenuations Measurement

Danasabe GAMBO[1*], Isyaku YA'U[2], Tisan A. GREGORY[3]

[1*]Department of Electrical Electronics Engineering, Kaduna State University, Kaduna, Kaduna State, Nigeria
[2]Department of Electronics and Telecommunications Engineering, Ahmadu Bello University, Zaria, Nigeria
[3]Department of Electrical Electronics Engineering Technology, Nuhu Bamalli Polytechnic, Zaria, Kaduna State, Nigeria

[1*]danasabegambo@gmail.com, [2]isiyakuyau@abu.edu.ng, [3]gregoryakau@gmail.com

Abstract

This research developed a cost-effective laboratory testbed for Free Space Optical Communication (FSOC) that serves as an educational and research platform for studying modern optical communication. The system was designed to transmit both text and audio signals and its performance was experimentally evaluated under controlled fog and rain conditions. Two types of receivers were tested: a mini solar panel and a photodiode. Findings revealed that the solar panel consistently achieved higher SNR values of 60 dB in fog and 90 dB in rain compared to the photodiode, which attained 38 dB and 58 dB respectively, at the same BER of 10^{-4}. The superior performance of the solar panel is attributed to its larger field of view, which helps reduce beam divergence losses. Finally, the developed system demonstrated a bandwidth of 8.450 GHz, making it a useful educational and experimental platform for FSOC research.

Keywords: *Fog, rain, attenuation, SNR and bandwidth.*

1.0 Introduction

As technology continues to evolve, communication devices are becoming more sophisticated and widely used. This growing adoption has led to an increasing demand for higher data transmission rates as depicted in Table 1. This has resulted in spectrum congestion within Radio Frequency (RF) systems.

Table 1: Internet Demand Versus Years (ITU, 2025)

Year	Internet Users	Global Population on Internet (%)
1990	2.6×10^6	0.05
1995	39.2×10^6	0.7
2000	361×10^6	6.0
2005	1.0×10^9	15
2010	1.9×10^9	27
2015	3.0×10^9	40
2020	4.5×10^9	57
2025	5.6×10^9	68

In recent years, the communication industry has witnessed significant advancements (Kaushal and Kaddoum, 2016). The rapid growth in fast internet usage, video conferencing, and live streaming has drastically increased the global need for bandwidth. Reports indicate that more than 70% of the world's population was projected to have internet access by 2025, driven by continuous progress in the electronics and telecommunications sectors (Saiyyed, 2024). Accordingly, the number of internet users was expected to grow from about 2.1 million (0.05%) to approximately 5.7 billion (68%) by 2025 (ITU, 2025), as shown in Figure 1.

Received: 16/11/2025; Revised: 08/12/2025; Accepted: 08/12/2025; Published: 22/12/2025

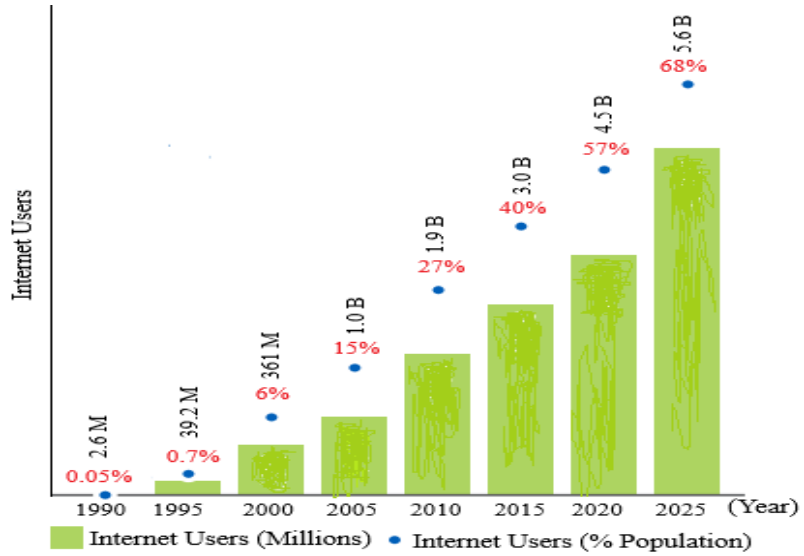

Figure 1: World Internet Users Growing (ITU, 2025)

In Nigeria, the Nigerian Communications Commission (NCC) estimated the country's broadband-penetration at 33% in 2018 (NCC, 2020). On a global scale, there were about 4.8 billion internet users by the second quarter of 2020, marking a 1,239% increase between 2000 and 2021 (NCC, 2020). The continuous rise in internet usage and the demand for higher bandwidth, driven by emerging digital applications, have led to increasing pressure on the conventional Radio Frequency (RF) spectrum. This growing constraint has prompted the search for alternative communication technologies to complement or replace traditional RF systems.

To address this challenge, researchers are exploring alternative technologies capable of supporting greater data capacity.

One of the most promising alternatives is Free-Space Optical Communication (FSOC), alongside technologies such as massive MIMO and cognitive radio networks. FSOC transmits data using optical carriers through the atmosphere without the need for guiding media. It offers broad bandwidth and high data rates, making it suitable for multimedia and high-speed communication applications (Mingjian et al., 2018). Nevertheless, the performance of FSOC systems is highly sensitive to atmospheric disturbances, including fog, rain, snow, clouds, wind, dust, and aerosols, which cause scattering, absorption, and turbulence leading to signal attenuation.

This research focuses on mitigating the impact of fog—one of the most detrimental atmospheric factors—on FSOC performance through mathematical modeling and machine learning-based simulations.

2.0 Related Work

Kashani et al. (2015) explained that FSOC networks are significantly influenced by atmospheric temperature variations, which fluctuate across all the spatial and equally with temporal areas. Esmail *et al.,* (2016) established a combined fog attenuation model for FSOC networks, while Henniger and Wilfert identified fog, dust, and rain as the primary factors responsible for signal degradation in FSOC channels. Farouk *et al.* investigated the performance of FSOC systems under fog conditions using Kruse's and Kim's models equations, whereas Jahid *et al.,* conducted a comprehensive investigation on FSOC devices, exploring it potentials and technical issues. In a related study, Gambo et al. (2023) explored the reduction of beam divergence losses in FSOC systems by employing a field-of-view (FOV) approach. Recent studies show that rain significantly weakens FSOC links. Attri et al. (2024) reported severe signal loss in 4QAM-OFDM-FSO systems during rainfall, while Djir et al. (2023) observed notable image degradation. Zabidi found that tropical high-intensity rain causes strong attenuation and reduced link availability. The Al-Iraqia study confirmed that rain degrades both optical and 58 GHz channels in hybrid systems. Ojo et al. (2025) concluded that although fog is more attenuating per kilometer, frequent heavy rainfall remains a major limitation in tropical FSOC environments.

2.1 Technical Challenges

Although FSOC offers numerous benefits, its large-scale implementation is limited by several technical constraints, including absorption, scattering, and signal distortion. Since FSOC relies on free space as its transmission medium whose characteristics vary unpredictably with both space and time, the system's performance is highly sensitive to atmospheric conditions and geographical location. This behavior, depicted in Figure 2, reflects it random nature of propagation (Kedar and Arnon, 2004)

Received: 16/11/2025; Revised: 08/12/2025; Accepted: 08/12/2025; Published: 22/12/2025

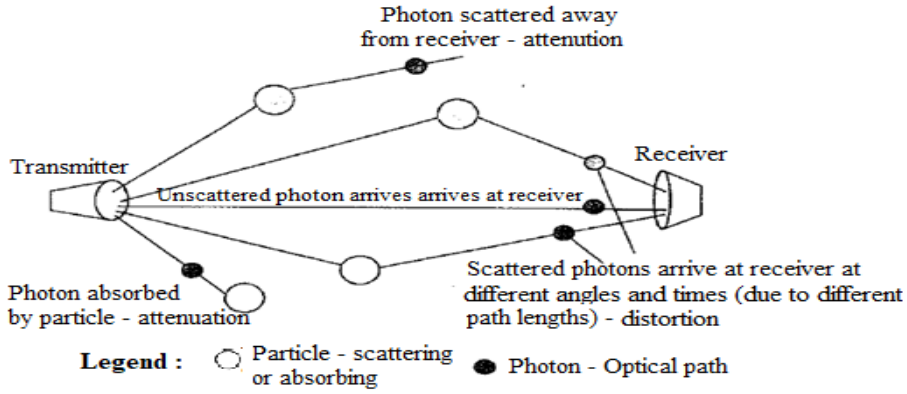

Figure 2: Angular and Spatial Dispersion and Change in Photon Pathway (Kedar and Arnon, 2004)

2.2 Absorption and Scattering

The attenuation encountered in Free-Space Optical Communication (FSOC) systems primarily arises from absorption and scattering mechanisms within the atmosphere. In the visible and infrared (IR) wavelength range, the principal atmospheric absorption agents are water vapor, carbon dioxide (CO_2), and ozone (O_3) (Ijaz et al., 2013a). The attenuation encountered by an optical signal as it travels through the atmosphere can be evaluated using the optical depth (τ), which defines the relationship between the received optical power (P_n) and the transmitted optical power (P_t) (Fang et al., 2018). This relationship is mathematically represented as:

$$P_R = P_T \exp(-\tau) \quad (1)$$

Where: τ is the ratio of the optical power received to that of optical power transmitted in FSOC network. This is known as transmittance. Mathematically expressed as (Ijaz et al., 2013b):

$$T_a = P_R/P_T = \exp(-\tau) \quad (2)$$

where T_a is the transmittance and τ is the optical depth.

Equations (3) and (4) relays the attenuation coefficient γ and the propagation distance (Range) R as in (Ijaz *et al.,* 2013b):

$$T_a = exp\left(\int_0^R (\rho) d\rho\right) \quad (3)$$

$$\tau = \int_0^R \gamma(\rho) d\rho \quad (4)$$

The loss, expressed in decibels (dB), experienced by the optical signal as it propagates through the atmosphere is defined by Equation (5). (Lin, 2024).

$$LOSS_{prop} = -10\log_{10} T_a \quad (5)$$

3.0 Research Method

The key objective of this study is to develop FSOC testbed and also to validate the fog attenuation model specifically suited for tropical climatic conditions. The subsequent section presents a systematic, step-by-step description of the methodology employed to achieve this objective

3.1 Fog Attenuation Modeling

Fog consists of suspended water droplets that greatly reduce visibility near the ground, typically to about 1 km (Ijaz et al., 2012). These droplets scatter and absorb optical signals, thereby limiting the effective FSOC link range to around 0.5 km. Theoretically, fog attenuation is analyzed by assuming spherical droplets and applying Mie scattering theory to determine their effect on signal propagation.

phenomenon over the cross-sectional area (C_s) of a particle, given its radius (r). Accordingly, the normalized scattering efficiency (Q_s) can be estimated using Equation (6) (Shaker and Ali, 2019) as:

$$Q_s = \frac{C_S}{\pi r^2} \quad (6)$$

The attenuation of optical signals in the atmosphere arises from the combined effects of molecular absorption and light scattering. In Free-Space Optical Communication (FSOC) systems, however, the operating wavelengths are typically chosen within atmospheric transmission windows to minimize molecular absorption losses. Consequently, the optical attenuation βλ resulting from fog-induced scattering can be expressed as (Shaker and Ali, 2019):

Received: 16/11/2025; Revised: 08/12/2025; Accepted: 08/12/2025; Published: 22/12/2025

$$\beta_\lambda = \int_0^\infty \pi r^2 Q_S\left(\frac{2\pi r}{\lambda}, n'\right) n(r) dr \qquad (7)$$

where n'n'n' represents the real part of the refractive index, n(r)n(r)n(r) denotes the particle size distribution, and λ\lambdaλ is the operating wavelength.

Fog particles are randomly distributed in the atmosphere, making fog attenuation difficult to estimate due to variations in particle size and distribution. Hence, empirical models using visibility data are commonly employed. The meteorological visibility or visual range (v) is the main parameter for analyzing fog attenuation, expressed using the Koschmieder law (Flecker et al., 2015),

$$V = \frac{10 \log_{10} T_{th}}{\beta_\lambda} \qquad (8)$$

where T_{th} is visual threshold

Kruse proposed an empirical model that relates visibility (v), attenuation coefficient (βλ), and wavelength (λ) to simplify the evaluation of fog attenuation by avoiding the complexities of particle size and distribution analysis. The attenuation caused by fog is influenced by both the wavelength of the optical signal and the existing visibility conditions. Thus, fog attenuation can be estimated using the empirical formula presented in [23].

$$\beta_\lambda = \frac{10 \log_{10} T_{th}}{V}\left(\frac{\lambda}{\lambda_o}\right)^{-q} \qquad (9)$$

λ is the wavelength, while λ₀ denotes the peak wavelength of the solar spectrum (550 nm), q is the particle size distribution coefficient as defined by Kruse (Killinger, 2002) as expressed in equation (10).

$$q = \begin{cases} 1.6 & \text{for v} > 50 \text{ km} \\ 1.3 & \text{for } 6 < v < 50 \text{ km} \\ 0.585(\text{V})^{1/3} & \text{for } 0 < v < 6 \text{ km} \end{cases} \qquad (10)$$

The parameter *q* in equation (10) is derived from the characteristics of haze particles in the atmosphere. As a result, the Kruse model tends to yield less accurate estimations. To correct this limitation, Kim improved the Kruse model by adjusting the *q* values, as presented in equation (11) (Adel et al., 2020).

$$q = \begin{cases} 1.6 & \text{for v} > 50 \text{ km} \\ 1.3 & \text{for } 6 < v < 50 \text{ km} \\ 0.16V + 0.34 & \text{for } 1 < v < 6 \text{ km} \\ \text{v} - 0.5 & \text{for } 0.5 < v < 1 \text{ km} \\ 0 & \text{for v} < 0.5 \text{ km} \end{cases} \qquad (11)$$

The combination of equations (9) and (11) shows that the attenuation coefficient (β_λ) is not dependent on wavelength when visibility (*v*) is below 0.5 km, where *q* equals 0 (Adel et al., 2020). Nevertheless, optimizing the related parameters under low-visibility conditions for the new *q* value is necessary to further minimize attenuation effects resulting from channel impairments.

3.2 Modelling and Simulation

Kim's modification of the Kruse model, as shown in (11), revealed that the attenuation coefficient (β_λ) remains independent of wavelength when visibility $\text{v} < 0.5$ km. However, as visibility decreases for any incident wavelength λ_{nm},, the value of *q* may vary by a factor *X(v)*. Consequently, it becomes essential to revise the existing models by introducing a buffer region for *q*, to further analyze and enhance the model's performance, especially under low-visibility conditions (v < 0.5 km), as illustrated in (12).

$$q = \begin{cases} 1.6 & \text{for V} > 50 \text{ km} \\ 1.3 & \text{for } 6 < V < 50 \text{ km} \\ 0.16V + 0.34 & \text{for } 1 < V < 6 \text{ km} \\ \text{V} - 0.5 & \text{for } 0.5 < V < 1 \text{ km} \\ \text{X(V)} & \text{for V} < 0.5 \text{ km} \end{cases} \qquad (12)$$

To implement the planned modification, it is necessary to examine more closely the interdependence of the Kruse's model variables in Equation (9)—notably the visibility, attenuation, particle size distribution (q), and the optical wavelength within the relevant solar spectrum. This analysis should proceed under a clear set of assumptions as:

i) Attenuation considered to be constant
ii) λ is also constant

Hence,

Received: 16/11/2025; Revised: 08/12/2025; Accepted: 08/12/2025; Published: 22/12/2025

$$V = a\left(\frac{\lambda}{\lambda_o}\right)^{-q} \quad (13)$$

$$a = \frac{10\log_{10} T_{th}}{\beta_\lambda} \quad (14)$$

The proposed model equation can therefore be expressed as shown in (15)

$$ln\, V = ln\, a + q ln\left(\frac{\lambda_o}{\lambda}\right) \quad (15)$$

Equation (15) represents the linearized form of equation (9). Accordingly, the cost or error function is defined as follows:

$$\mathrm{v}\left(\left(\frac{\lambda_\mathrm{o}}{\lambda}\right), \mathrm{k}\right) = \frac{1}{\mathrm{n}}\sum_{\mathrm{i}=1}^{\mathrm{n}}\left[\mathrm{v}_i - \left(\left(\frac{\lambda_\mathrm{o}}{\lambda}\right)_\mathrm{i} + \mathrm{k}\right)\right]^2 \quad (16)$$

In the Gradient Decent Optimization (GDO) method, the parameter k, and the ratio $\left(\frac{\lambda_\mathrm{o}}{\lambda}\right)$ of equation (16) correspond to the bias (B) and weight (W). These refer to the iteration indices of the optimization procedure. The weight and bias parameters—given in (17) and (18)—are extracted during training and used to form the trained model equation. Therefore, the objective functions are defined as: (i) Loss < 0.5 and (ii) v < 0.5 km. This ensures that the predicted visibility value (vp) does not exceed 0.5 km. Likewise, maintaining a loss function value below 0.5 guarantees improved accuracy of the results.

3.3 Solving the Optimization Problem

The Gradient Descent Optimization (GDO) technique was adopted in this research as the primary optimization approach. This technique possesses the capability for automated reasoning to determine the best-fit solution. Additionally, it includes a convergence control parameter, known as the learning rate, which regulates the speed of convergence during the optimization process. GDO effectively handles both linear and nonlinear functions, utilizing momentum to enhance stability and convergence in complex functions. It operates by applying an update rule to adjust model parameters iteratively throughout the automated learning process.

In this research, the technique is considered from the fundamental calculus perspective, with the update rules expressed in equations (17) and (18), which are used to guide the iterative optimization process (Garcia, 2018) as:

$$W = W - \mu \dot{hf}(L) \quad (17)$$

$$B = B - \mu \dot{hf}(L) \quad (18)$$

Where: $W\ is\ the\ weight, B\ is\ the\ bias,$

μ is the learning rate and $\mathrm{h\dot{f}(L)}$ is first derivative of loss function

3.3.3 Python Programming Language

Python is an object-oriented language ideal for quickly designing and implementing technical and scientific applications. It provides seamless integration with various operating system calls and libraries, making it highly adaptable for diverse computational tasks. Its high-level syntax, combined with efficient execution speed, makes Python both convenient and user-friendly for researchers and developers. These features make it particularly suitable for implementing the Gradient Descent Optimization (GDO) technique effectively and efficiently.

3.4 Experimental Measurement

The FSOC testbed was effectively built, as illustrated in Figure 3. Artificial fog was produced using a fog machine, after which the optical signal was transmitted from the constructed optical-transmitter and received by the optical-receiver at varying distances. This procedure was repeated multiple times to ensure measurement consistency. During each test iteration, the voltage / current sensors documented the corresponding values, which were subsequently stored on an SD card for further analysis.

Received: 16/11/2025; Revised: 08/12/2025; Accepted: 08/12/2025; Published: 22/12/2025

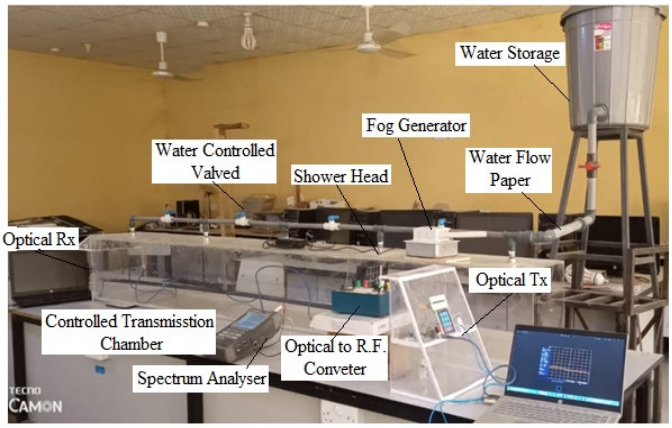

Figure 3: Constructed Test-bed illustration

3.4.1 Optical Transmitter

The transmitter accepts an electrical input signal, processes it, and converts it into an optical signal. Optical sources like Light Emitting Diodes (LEDs) or laser diodes are typically utilized to generate the optical signal for propagation through a free-space optical medium. In an Arduino-based optical transmitter, the Arduino generates and modulates an electrical signal to drive a LED or laser diode, converting the data into a light beam. The light is then directed toward the receiver, with the Arduino controlling parameters like transmission speed, pulse duration, and modulation for reliable short-range optical communication. illustrated in Figure 4.

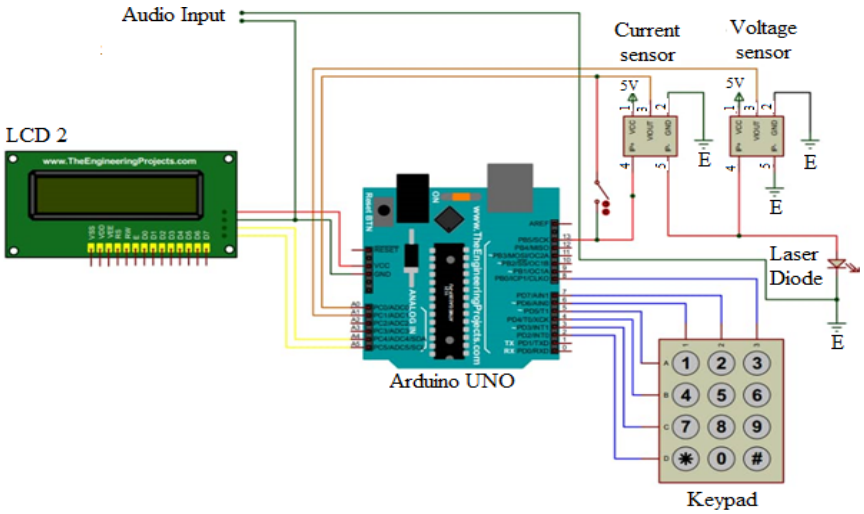

Figure 4: Optical Transmitter Circuit

3.4.2 Optical Receiver

In FSOC systems, the receiver commonly uses a photodiode to detect the optical signal sent from the transmitter. However, the limited aperture of the photodiode often results in substantial optical power loss due to beam divergence over the transmission path. To address this limitation, a mini solar panel—with a larger receiving area than the photodiode—was utilized as the optical detector. The circuit diagram of the developed optical receiver is illustrated in Figure 5.

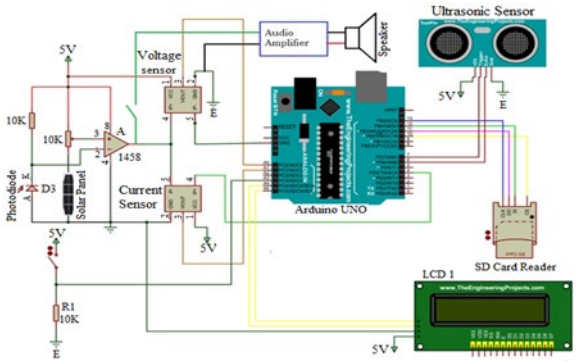

Figure 5: Optical Receiver Circuit

Received: 16/11/2025; Revised: 08/12/2025; Accepted: 08/12/2025; Published: 22/12/2025

In an Arduino-based optical receiver, a photodiode or light sensor detects the incoming modulated light from the transmitter and converts it back into an electrical signal. The Arduino reads this signal, demodulates it, and processes the data for display, storage, or further control, with the microcontroller handling timing, decoding, and error correction for reliable short-range optical communication.

4.0 Results and Discussion

This section presents the simulation and optimization results for the Kim, Kruse, and the proposed enhanced fog attenuation models. The comparison focuses on their performance in FSOC channels under low-visibility conditions. Results show that the improved model significantly reduces attenuation compared to the existing ones.

4.1 Optimization of the Developed Model at Low Visibility ($V \leq 0.5$ km)

The model formulated in Equation (15) was subsequently refined and optimized, as represented in Equation (20). This optimization aims to enhance the model's predictive capability by maximizing the particle size distribution coefficient (q) under low-visibility conditions. Figure 6 illustrates how visibility varies with the particle size distribution coefficient (q) in the optimized model.

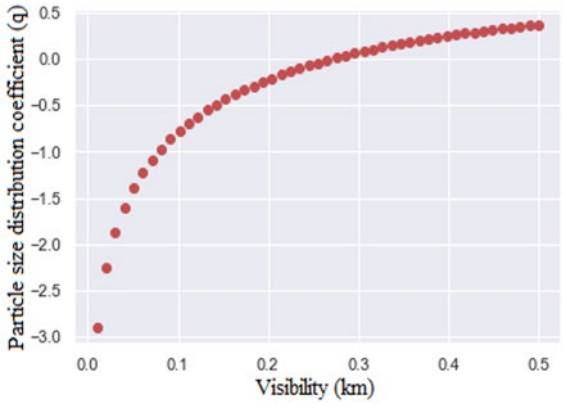

Figure 6: Particle Size Distribution Coefficient (q) Versus Low Visibility ($V \leq 0.5$ Km) of the Established Model

As shown in Figure 6, the optimization results indicate that the particle size distribution coefficient (q) was effectively increased to values above zero under low-visibility conditions (v < 0.5 km). Additionally, the developed model achieved an improvement of about 0.4 in the maximum q value compared to the results obtained from the Kim and Kruse models, as depicted in Figure 5.

4.2 Determination of the Optimized empirical model at low visibility ($V \leq 0.5$ km)

The weights and biases presented in Equations (17) and (18) were evaluated using an empirical method to derive the optimized model that accurately fits the optimization curve shown in Figure 8. The Python optimization code provided in Equation (19) demonstrates the correlation among the weight (W), bias (B), and particle size distribution coefficient (q).

$$\text{Outputs} = \text{Weight} * \text{np.log(inputs)} + \text{Bias} \quad (19)$$

In this context, the output corresponds to the particle size distribution coefficient (q). After calculating the weight and bias values, they were substituted into Equation (19) to obtain the optimized empirical model presented in Equation (20).

$$q = 0.773429 \ln(v) + 0.9074367 \quad (20)$$

Equation (20) expresses the optimized empirical model that closely fits the curve displayed in Figure 9. Table 1 provides the computed optimized values of the particle size distribution coefficient (q) together with their respective visibility values.

Table 2: Optimized Particles Size Distribution Coefficients against Visibility

S/N	Particles size distribution coefficients (q)	Visibility (km)
1	-0.87305488	0.1
2	-0.32520539	0.2
3	0.00473399	0.3
4	0.20107098	0.4
5	0.39901224	0.5

Received: 16/11/2025; Revised: 08/12/2025; Accepted: 08/12/2025; Published: 22/12/2025

4.3 Improved Model

Equation (20) defines the developed empirical model describing the particle size distribution coefficient (q) under low-visibility conditions. Hence, it functions as a visibility-based expression applicable for v < 0.5 km. Subsequently, Equation (21) shows the modified Kim model derived from Equation (11).

$$q = \begin{cases} 1.6 & \text{for v} > 50 \text{ km} \\ 1.3 & \text{for } 6 < v < 50 \text{ km} \\ 0.16v + 0.34 & \text{for } 1 < v < 6 \text{ km} \\ \text{v} - 0.5 & \text{for } 0.5 < v < 1 \text{ km} \\ 0.773429 \ln(v) + 0.9074367 & \text{for v} < 0.5 \text{ km} \end{cases} \quad (21)$$

4.4 Comparing Models

Figure 10 illustrates the comparative performance of the three (3) models in terms of attenuation versus visibility. The particle size distribution coefficient (q) is defined for the Kruse and Kim models by Equations (10) and (11), respectively, while the improved model introduces a new expression for (q) at low visibility, as shown in Equation (21). To assess the level of improvement, a visibility value of 0.25 km was selected to calculate the percentage reduction in attenuation achieved by the improved model relative to the existing ones, as detailed below:

$$\text{Improve/Kruse Models} = \frac{32 - 20}{32} = 37.5\ \%$$

$$\text{Improve/Kim Models} = \frac{30 - 20}{30} = 33.33\ \%$$

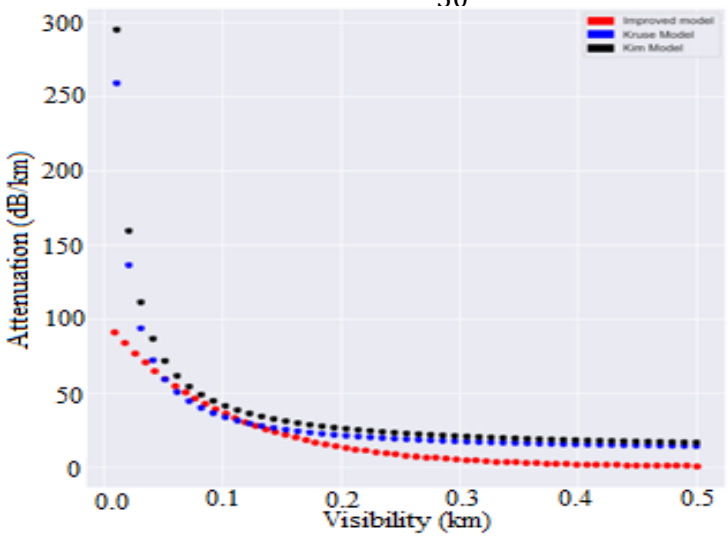

Figure 7: Attenuation at Low Visibility of the Developed in Comparison with the Other Models

Figure 7 shows that the Kim and Kruse models display behavior similar to the proposed improved model for visibility values of v ≤ 0.5km. However, the improved model performs notably better by producing lower attenuation levels than the existing ones. At a visibility of 0.01 km, for example, the improved model yields an attenuation of about 100 dB/km, while the Kruse and Kim models produce significantly higher values—around 3000 dB/km. Additionally, Figure 8 indicates that the improved model aligns more accurately with the measured training data than the other models.

Received: 16/11/2025; Revised: 08/12/2025; Accepted: 08/12/2025; Published: 22/12/2025

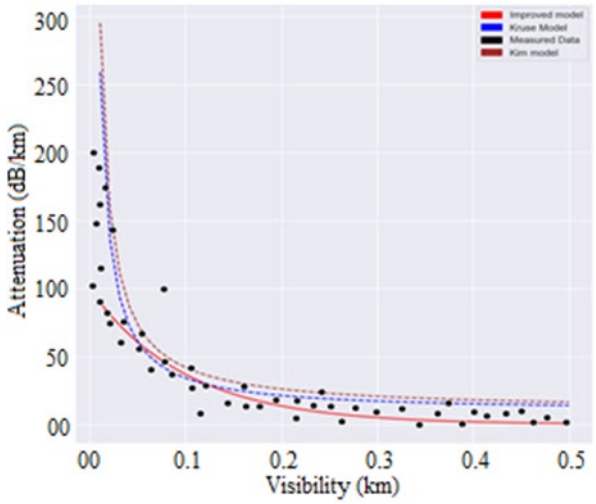

Figure 8: Measured of Fog Attenuation Coefficient as a Function of Visibility.

4.5 Rain

As already discussed in section two of this report, during the period of rainfall, the particles of the rain affect the optical signal propagation causing distortion in the FSOC link. Consequently, there is a need to study and evaluate how the rain particles affect the signal for possible improvement. Therefore, some water sprinklers (shower heads) were included in the testbed construction to imitate or create artificial rain in a controlled manner. Measurements were taken under artificial rain condition and the data obtained were trained and the best fit curve was obtained using machine learning. Similarly, the existing rain (Kaushal) Model as in equation (2.18) was replicated and compared with the trained model as demonstrated in Figure 9.

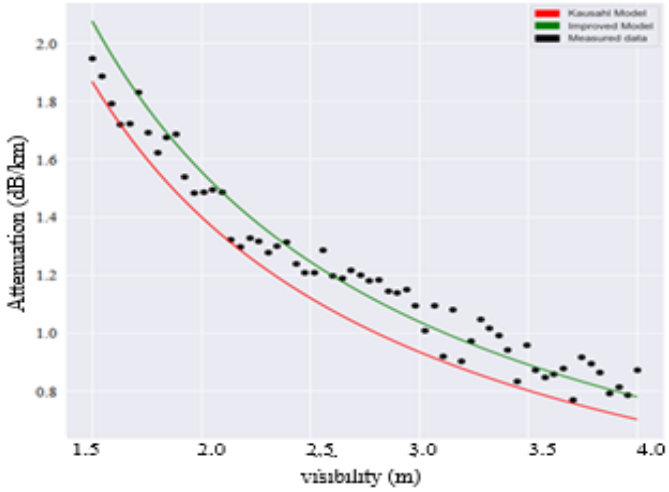

Figure 9: Measured, Kaushal and developed Rain Models as a Function of Visibility

Figure 12 shows both the existing (Kaushal rain model) and the trained (developed) model. The measured data were trained using machine learning algorithm. The best fit curve was obtained and the trained model equation was derived through weight and bias estimation. Consequently, the developed model equation is given by:

$$\beta_{\text{rain new}} = \text{Weight}\left(\frac{1}{\text{v}}\right) + \text{Bias} \qquad (22)$$

where, v is the visibility, Weight is the gradient and Bias is the intercept.
Therefore, by substituting the estimated values of the weight and bias, the numerical model equation becomes.

$$\beta_{\text{rain new}} = 3.1\left(\frac{1}{\text{v}}\right) + 0.025 \qquad (23)$$

4.7 BER Against SNR for Fog Measurement

Signal-to-Noise Ratio (SNR) measures the quality of a communication signal by comparing the power of the signal to that of the noise. A higher SNR indicates better signal clarity and reliability. In this study, SNR was used to assess the performance of the developed FSOC system under different atmospheric conditions. Experiments were performed using the developed testbed in an artificial fog environment across varying transmission distances. A photodiode and a mini solar panel were each used separately as optical detectors. The obtained measurement

Received: 16/11/2025; Revised: 08/12/2025; Accepted: 08/12/2025; Published: 22/12/2025

data were then analyzed to model the relationship between the Bit Error Rate (BER) and the Signalto-Noise Ratio (SNR), as shown in Figure 10.

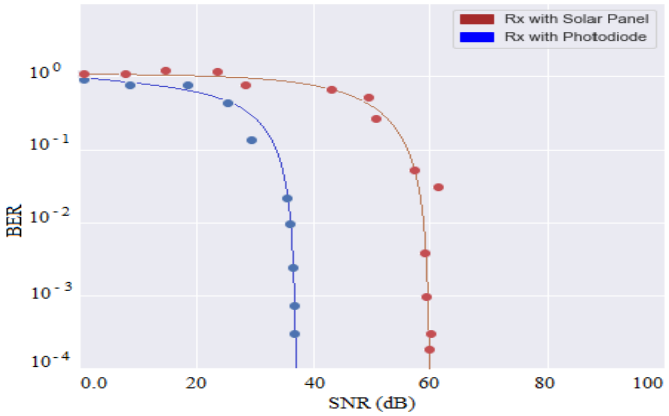

Figure 10: BER Against SNR for Fog Measurements

Figure 10 shows that as the Signal-to-Noise Ratio (SNR) increases, the Bit Error Rate (BER) decreases, indicating an inverse relationship. The solar panel receiver outperformed the photodiode, achieving an SNR of about 60 dB at a BER of 10^{-4}, while the photodiode recorded around 38 dB due to beam divergence losses from its narrow field of view.

4.8 BER Against SNR for Rain Measurement

The experimental process used for fog measurements was similarly conducted under simulated rain conditions, as shown in the testbed setup. The recorded data from these experiments were subsequently used to establish and plot the relationship between the Bit Error Rate (BER) and the Signal-to-Noise Ratio (SNR). Ratio (SNR), as presented in Figure 11.

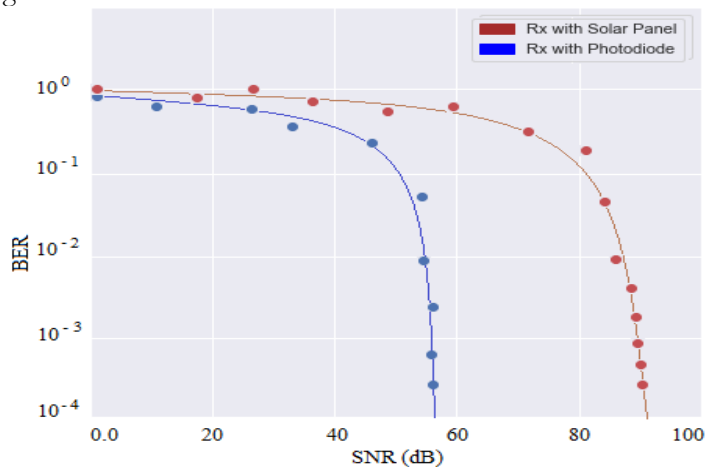

Figure 11: BER Against SNR for Rain Measurements

Figure 11 shows that the photodiode receiver achieved an SNR of 57 dB at a BER of 10^{-4}, while fog conditions reduced it to 38 dB at the same level. This confirms that fog causes greater attenuation than rain. Using a mini solar panel as the receiver minimized beam divergence losses due to its wider field of view.

4.9 Bandwidth Estimation

Optical signals offer high bandwidth capacity, making FSOC a strong alternative to conventional RF networks. Bandwidth evaluation is one of the key performance metrics in this study. Figure 12 shows the output spectrum from the analyzer, indicating the achieved bandwidth of the system.

Received: 16/11/2025; Revised: 08/12/2025; Accepted: 08/12/2025; Published: 22/12/2025

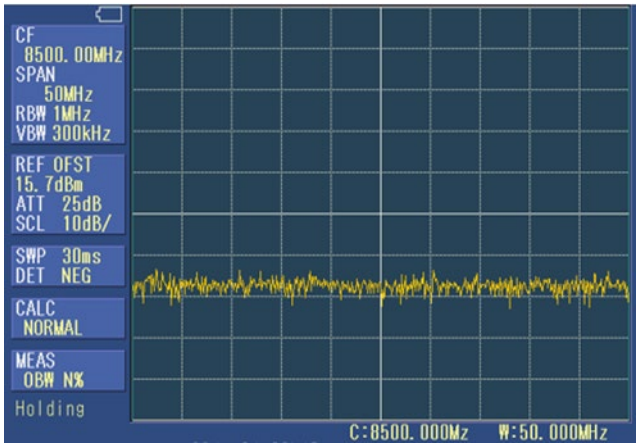

Figure 12: Optical Bandwidth Estimation

Figure 12 is the plot of the spectrum analyze whereby the values of upper and lower frequencies were evaluated. Consequently, the bandwidth of the system was estimated using equation (24) as:

$$\text{Bandwidth } (B) = f_H - f_L \qquad (24)$$
$$\text{Bandwidth } (B) = 8500\ MHz - 50MHz$$
$$\text{Bandwidth } (B) = 8.450\ GHz.$$

5.0 Conclusion

This research focuses on validating a fog attenuation model tailored for tropical regions. Improved models were developed, optimized, and simulated with the aim of identifying the most suitable parameters and confirming the accuracy of the proposed model. Comparison with existing models showed that the new model achieved attenuation reductions of 33.33% and 37.5% relative to the Kim and Kruse models, respectively. Within the visibility range of 0.3 < V < 0.5 km, the optimal q values were found to be 0.00473399, 0.20107098, and 0.39901224, obtained by maximizing the particle size distribution coefficient. The developed model exhibited a strong correlation with experimental data, validating its effectiveness. Further investigations are suggested for lower visibility conditions (0 < V < 0.2 km) to enhance model performance and further minimize fog-induced attenuation

References

Adel M., Seleem H., Nasr M., and El-Khobby., (2020), Transmission of 128 Gb/s Optical QPSK Signal over FSO Channel under Different Weather Conditions and Pointing Errors, Journal of Physics: Conference Series 1447 (2020) 012055, Tanta, Egypt. 1-7.

Al-Iraqia Journal for Scientific Engineering Research. (2024). *Impact of rain weather conditions over hybrid FSO/58 GHz communication link in tropical region. Al-Iraqia Journal for Scientific Engineering Research, 3*(3). (See full article for authors.) (Iraqi Academic Scientific Journals).

Attri, S., Madhu, C., & Kaur, D. (2024). *Performance analysis of 4QAM-OFDM- FSO link under rain weather conditions. Journal of Optical Communications*, (2), 421–431. https://doi.org/10.1515/joc-2024-0021 (OUCI).

Chowdhury Z. M., Shahjalal Md., Hasan K. M., and Jang M.Y., (2019) The role of optical wireless communication technology in 5G/6G and IoT solution: prospects, direction, and challenges Jour nal of applied science. (Appl. Sci. 2019, 9, 4367). pp. 1-20.

Cisco (2020), Cisco Annual Internet Report, 2018-2023,whitepaper,onbroadband, Wi Fi, and mobile (3G, 4G, 5G)networking ,pp.5 https://www.cisco.com/c/en/us/sol utions/collateral/executiveperspectives/a nnual-internet-report/white-paper.

Djir, A., Meskine, F., & Tayebi, M. L. (2023). *Rain effects analysis on image transmission through free space optical communication system. Journal of Optical Communications*, (s1), S2029–S2040. https://doi.org/10.1515/joc-2023-0165 (OUCI).

Gambo D., Tekanyi A.M.S., Musa M.J., Al-Mustapha M.D. and Ya'u I (2023) Beam Divergence Loss Mitigation in Free Space Optical Communication Channel Using Field of View Technique. Sule Lamido University Journal of Science & Technology Vol. 6 No. 1&2[March, 2023], 30-43. https://doi.org/10.56471/slujst.v6i.344. Online ISSN: 2736-0903, Print ISSN: 2736-089X, www.slujst.edu .ng

Esmail A. M., Fathallah H. and Alouini M., (2016), Analysis of Fog Effects on Terre strial Free Space Optical Communicatio n Links, *In: IEEE ICC 2016 Workshops: W02 Second*

Workshop on Optical Wireless Communications. King Abdulaziz City for Science and Technology (KACST), 34-45.

Fang J., Shilin M.B., Yang X.G., Liu L., Zhang Y., & Hu. W., (2018), Polar code MIMO FSO communication over gamma-gamma turbulence channel with spatial correlated fading. Journal of optical communication networks volume 10. No. 11. Optical society of America. pp. 915-923.

Farouk K., Shaker, and Ali M. A. A., (2019), Performance of Free Space Optical Communication Link under Foggy Weather, *In: Journal of Communications, 14(6),* Research Gate, 518-523.

Flecker B., Gebhart M., Leitgeb E., Muhammad S.S., and Chlestil C. (2015), Results of attenuation measurements for Optical Wireless channels under dense fog conditions. regarding different wavelengths, Proc. of SPIE Vol. 6303 pp1-11.

Garcia S. I., (2018) An introduction to Descent Algorithm, Computer science engineer and Machine Learning enthusiast Retrieved from https://medium.com/@montjoile on 20/10/20, at 2:.30pm.

Henniger H. & Wilfert O. (2010), An introduction to free space optical communication, journal of radio engineering, vol, 19, number 2, 203 – 212.

Ijaz M., Ghassemlooy Z., Perez J., Brazda V., and Fiser O. (2013a), Enhancing the Atmospheric Visibility and Fog Attenuation Using a Controlled FSO Channel, IEEE, Photonics Technology Letters, Vol. 25, No. 13, 2013.Pp 1262 – 1265.

Ijaz M., Ghassemlooy Z., Rajbhandari S., Le Minh H., Perez J., and Gholami A., (2012), Comparison of 830 nm and 1550 nm based Free Space Optical link under Controlled Fog Conditions, 8th IEEE, Internation-al Symposium on Systems, Networks and Digital Signal Processing, pp 4577-1473.

Ijaz M., Ghassemlooy1 Z.., Le-minh H., Zvanovec S., Perez J., Pesek J., and Fiser O., (2013b), Experimental Validation of Fog Models for FSO under Laboratory Controlled Conditions, 2013 IEEE 24th International Symposium on Personal, Indoor and Mobile Radio Communications: Fundamentals and PHY Track, pp.19-23.

International Telecommunication Union (ITU), (2025), outlined the trajectory of the growth of the Internet in the world from 1994 to 2021.

Jahid A., Alsherif M. H., and Hall T.J., (2022), A contemporary survey on free space optical communicatin: Potential, technical challenges, recent advances and research direction,Journal of network and comp uter applications, Science Direct, Elsevier, doi.org/10.1016/j.jnca.2021.103311. 200 (22), 15-22.

Kashani M.A., Uysal M., and Kavehrad M., (2015), A novel statistical channel model for turbulence-induced fading in free- space optical systems, *In: Journal of Light wave Technology.* IEEE, 1-10.

Kaushal H., Jain, V. K., & Kar, S., (2017). Free Space Optical Communication, Opt ical Networks, Springer (India) Pvt. Ltd. DOI 10.1007/978-81-322-3691-7. Pp. 41-49.

Kaushal H. and Kaddoum G. (2016), Optical Communication in Space: Challenges and Mitigation Techniques. In Communications Surveys & Tutorials. pp. 1-41. IEEE.

Kedar D. and Arnon S. (2004). Urban optical wireless communication networks: the main challenges and possible solution. In Journal of Optical communication, pp. 52-57. IEEE.

Khalid H. S., Neil J.M., Peter S.E., Raed A.A., and Chan H. S., (2019) Antenna for emerging 5G system. In International jo urnal of antenna and propagation pp 1-3.

Killinger D., (2002). Free space optics for laser communication through the air. In *Optics & Photonics News,* vol. 13, pp. 36-42.

Lin, H.-M., Wang, C.-P., Lu, H.-H., Hayle, S. T., Huang, X.-H., Hsu, W.-W., Chung, Y.-C., Bai, Y.-Y., Okram, K., & Lu, J.-M. (2024). Bidirectional wavelength-division-multiplexing fibre-free-space optical communications using polarization multiplexing technique and tunable optical vestigial sideband filter. *Commun Eng, 3*, 128. https://doi.org/10.1038/s44172-024-00277-2 (PMC).

Mingjian, C., Y., G., Jiangting, L., Xiaotong, Z., And Lixin G., (2018), Inverse Gaussian gamma distribution model for turbulence induced fading in free space optical communication. In Applied Optics, Vol. 57, No. 12 / 20, Optical Society of America, pp3031-3037.

Nigerian Communication Commission (NCC) (2020). An exploratory study on the challenges and survivability of ISP licensees in the Nigerian telecom se ctor, pp.5-5. Availableat https://www.nc c.gov.ng/accessible/documents/978-study on the-challengesandsurvivabilityofisplicensees-in- the-nigerian-telecom-sector/file Retrieved on 21-05-21.

Ojo, O., et al. (2025). Fog and rain attenuation characterization and performance of terrestrial free space optical communication in Akure, Nigeria. Aptikom Journal on Computer Science and Information Technologies. (See full article for volume/issue.) (Aptikom Journal).

Patnaik S., Srujanika S. S., Anshuman P., Chandni J., (2016), Free Space Optical Communication,A Review. In International Research Journal of Engineering and Technology (IRJET), Volume: 03, Issue: 04. pp 1261-1265.

Qadir Z., Saeed N., Munawar H.S. (2021), Towards 6G Internet of Things: Recent Advances, Use Cases, and Open Challenges. www.sciencedirect.com, 2022. Pp. 1-16.

Rockwell D. A., & Mecherle G. S., (2001), Optical wireless: low cost high speed op tical access Asia-pacificoptical and wireless communications conference and exhibit, volume 4586, pp.11-15. Retriev ed fromhttps://www.spiedigitallibrary.or g/conference-proceedings-of-spie. On 04/02/20.

Saiyyed, R., Sindhwani, M., Ambudkar, B., Sachdeva, S., & Kumar, M. (2024). Free space optical communication system: A review of practical constraints, applications, and challenges. *Journal of Optical Communications*. https://doi.org/10.1515/joc-2024-0011 (Bohrium).

Shaker F. K., and Ali M. A. A. (2019), Performance of Free Space Optical Communication Link under Foggy Weather, Journal of Communications Vol. 14, No. 6, June 2019, pp.518-523.

Zabidi, S. A., Islam, M. R., Al-Khateeb, W., & Naji, A. W. (2024). *Analysis of rain effects on terrestrial free space optics based on data measured in tropical climate. IIUM Engineering Journal.* https://doi.org/10.31436/iiumej.v12i5.232 (IIUM Journals).

Received: 16/11/2025; Revised: 08/12/2025; Accepted: 08/12/2025; Published: 22/12/2025